Chemistry Africa (2024) 7:1595–1604
https://doi.org/10.1007/s42250-023-00824-y

ORIGINAL ARTICLE

# Chemically Functionalized Graphene–Boron Nitride/Polypropylene Nanocomposites with Enhanced Nanomechanical and Anti-wear Properties

**Uwa O. Uyor[1,3] · Abimbola P. I. Popoola[1] · Olawale M. Popoola[2,3]**

Received: 31 July 2023 / Accepted: 30 October 2023 / Published online: 25 November 2023


**Abstract**
Polymers are soft materials with large molecular chains, which are softened during frictional wear, leading to bulk detachment of materials and poor wear resistance in addition to their low mechanical strength and hardness. This study developed polypropylene nanocomposites containing hydrothermal assembled graphene and boron nitride (BN@GNs) with good mechanical properties and wear resistance. To ensure good dispersion of the nanoparticles in the polypropylene (PP) matrix, they were functionalized and preparation of masterbatch using polypropylene maleic anhydride (PPMA) was adopted, while the polymer nanocomposites for this study were developed via melt compounding. The addition of the nanoparticles in the PP matrix promoted its wear resistance as all the developed nanocomposites showed a low coefficient of friction (CoF). The wear rate of the nanocomposites was dramatically reduced to a minimum of $2.05 \times 10^{-4}$ mm$^3$/Nm for the PP/3wt%BN@GNs nanocomposite from around $24.9 \times 10^{-4}$ mm$^3$/Nm for the pure PP. The nanoindentation test results of the nanocomposites also revealed improvement in their nanomechanical characteristics. For instance, PP/3wt%BN@GNs nanocomposite showed an ideal increase of about 124% nano-hardness and 65.7% nano-elastic modulus when compared to pure PP. In comparison to pure PP, all of the developed nanocomposites displayed lower nano-percentage creep and nanoindenter's tip penetration depth, which suggest greater plastic deformation resistance.

**Keywords** Chemical functionalization · Wear · Nanomechanical · Polypropylene · Graphene and boron nitride

## 1 Introduction

Polymers are characterized by their high flexibility, elasticity, chemical resistance, toughness, storage modulus, lightweight, easy processing, and cost-effectiveness. With the rapid development in technology in the areas of aviation, aerospace and automobile, high-performance polymers are substituting the metallic materials as promising lubricating materials for tribological application [1]. Polypropylene (PP) is among the most important types of polymers (thermoplastics) used around the world due to their desired properties such as toughness, light weight, flexibility etc. [2]. Generally, polymers are soft materials with large molecular chains, which are softened during frictional wear due to poor heat management. Hence, this often results in bulk detachment of polymer from the bulk material under friction, resulting in poor wear resistance of polymers. In addition, the softness of polymer materials also leads to their low mechanical strength and hardness due to the fast and easy mobility of their molecular chains on the application of load [3]. However, the incorporation of nanofillers with the desired properties is one of the main strategies used by numerous studies to address the challenge of mechanical strength, thermal and tribological of polymers.

Various classes of nanofillers such as fibres and particulates with different dimensional structures have different ways or degrees of enhancing the mechanical properties of the polymer matrix. However, particulates-based polymer

✉ Uwa O. Uyor
UyorUO@tut.ac.za

[1] Department of Chemical, Metallurgical and Materials Engineering, Tshwane University of Technology, Pretoria, Private Bag X680, Pretoria, South Africa

[2] Department of Electrical Engineering, Tshwane University of Technology, Pretoria, Private Bag X680, Pretoria, South Africa

[3] Center for Energy and Electrical Power, Tshwane University of Technology, Pretoria, Private Bag X680, Pretoria, South Africa

composites seem to be more common and popular owing to their easy fabrication and suitability for the use of common techniques in fabrication such as extrusion, compression and injection moulding. Recently, the discovery of graphene nanosheets (GNs) has provided fresh perspectives to our understanding of nanomaterials with significant improvement in the materials in which it is incorporated [4]. GNs are planar sheets of $sp^2$-bonded carbon atoms that are one atom thick and tightly packed into a two-dimensional honeycomb crystal lattice [5]. To create polymeric materials with improved physicochemical features, such as mechanical and tribological properties [6], electrical and thermal conductivity, graphene has been combined with different polymers [2, 7]. Its significant contribution in promoting various polymers' properties even at very low concentrations is made possible by its large aspect ratio, high surface area, extremely small size, and hexagonal structure. By including GNs in the epoxy matrix, significant improvements in storage modulus, tensile modulus, and flexural modulus compared to pure epoxy have also been reported [8].

On the other hand, ceramic nanofillers are also an effective reinforcement phase in the enhancement of various properties of polymers including mechanical strength, hardness, anti-wear, etc. One such ceramic reinforcement is boron nitride (BN), which is characterized by its non-toxicity, wear resistance/lubrication, chemical inertness, and good mechanical properties [9]. In a study by Badgayan et al. [10], it was demonstrated that 0.1 wt% BN can lower the wear volume of high density polyethylene (HDPE) compared to when loaded with 0.1 wt% CNTs. The study further illustrated that the hybrid of 0.15 wt% BN and 0.25 wt% CNTs could further improve the wear response of the HDPE, where about 70% reduction in wear volume was recorded due to the lubricating effect of BN and high thermal conductivity of CNTs. Also, Songfeng et al. [11] demonstrated the positive effect of BN as a lubricant additive. The study overcome the challenge of interlayer interaction that exist between individual BN layer via hydroxylation and polydopamine modification, which gave good dispersion of the BN in water with improve wear resistance as a lubricant additive. Various other studies have used BN and GNs or a combination of both to promote and incorporate new properties in the polymer matrices. For instance, Madarvoni, Sreekanth [12] investigated the effect of GNs and BN nanoparticles on Kevlar and hybrid fiber-reinforced composites (FRP). Also, Jiang et al. [13] investigated functionalized GNs and BN synergistic influence on the thermal conductivity of polymer composites. They reported that the thermal conductivity of the composites reached a maximum enhancement of about 20% when the mass ratio of GN/BN-OH was 7:3.

Despite the reports on the use of hybrid GNs and BN in the improvement of various properties of polymers, limited works have been presented on the influence of the hybrid GN and BN on the tribological and nanomechanical properties of PP matrix for advanced engineering applications. Therefore, this study utilized these advanced engineering nanomaterials in developing PP nanocomposites with enhanced tribological and nanomechanical properties. This study further adopted surface functionalization of the nanoparticles and hydrothermal assembly to attached BN on the large surfaces of GNs (BN@GNs) and rapping of the BN@GNs with polypropylene maleic anhydrate (PPMA) before incorporating into the PP matrix via melt compounding. This approach promoted the dispersion of the nanoparticles in the PP matrix as layer-to-layer interactions of GNs was minimized by the presence of BN with significant enhancement in tribological and nanomechanical properties. The study showcased that BN@GNs could further enhance the tribological and nanomechanical responses of the nanocomposites compared to the use of GNs only. This study presents a further strategy to improve the properties of polymer materials for various advanced engineering applications.

## 2 Experimental Section

### 2.1 Materials

Hexagonal boron nitride (BN) (assay > 99.5%, particle size < 100 nm, and density of 2.2 g/mL at 25 °C) was provided by Hongwu International Group China. 3-glycidoxypropyltrimethoxysilane (GPTMS) (BP— 120 °C/2mmHg), xylene plus ethylbenzene basis (ACS reagent, essay > 98.5%), dopamine hydrochloride (DH) (essay > 98%, MW — 189.64, BP — 248–250 °C), polypropylene (PP) (density of 0.9 g/mL and a melt index of 4 g/10min at 230 °C/2.16 kg), polypropylene grafted maleic anhydride (PPMA) (0.5%, density of 0.92 g/mL), graphene nanosheets (GNs) (C > 95%, O < 3%, diameter — 2–3 µm, few nano thickness — 6–8 nm) were purchased from Sigma-Aldrich, South Africa.

### 2.2 Nanocomposites Functionalization and Preparation

To improve the interaction and dispersion of GN and BN in the PP matrix, the GNs' surface was modified using DH. Typically, 100 mL of distilled water was added to a beaker with 5 g of GNs mixed with it. The nanosheets were exfoliated by ultrasonically agitating the mixture for 4 h at 80 °C. To raise the pH of the suspension, 5 mL of ammonia solution was added after 5 g of DH was added to the mixture. While the DH was self-polymerized into polydopamine (PDA) in the presence of the GNs, the solution was left under ultrasonication for 10 h at 80 °C. The modified GNs were repeatedly rinsed to eliminate unpolymerized DH

after the process. On the other hand, GPTMS was used to modify the surface of BN. Using an ultrasonicator at 80 °C for 4 h, a hydrothermal technique was used to exfoliate the BN. A certain amount of BN was added to a beaker containing xylene with a slow addition of 100 mL of GPTMS. While the reaction took place, the mixture was ultrasonically treated for 10 h at 80 °C. The resultant surface-modified BN was then rinsed with distilled water after the procedure. In distilled water, functionalized GNs and BN were combined at a ratio of 3 wt%GNs to 15 wt%BN. For the hydrothermal assembly process to properly disperse the nanoparticles, the mixture was ultrasonically agitated for 4 h at 80 °C. The mixture was then covered with aluminum foil and kept in an oven for 10 h at 140 °C. The GNs and BN nanosheets were able to interpenetrate for the entire process. In this study, the attached BN onto GNs through this process is referred to as BN@GNs.

### 2.3 Nanocomposites Fabrication

PPMA compatibilizer and the nanoparticles were first used to make the masterbatch, which also helped to improve their compatibility and physical interaction with the PP matrix. 8%wt PPMA was dissolved in xylene at 140 °C for 30 min. The dissolved PPMA was then added to a beaker with a certain quantity of redispersed nanoparticles in xylene. The mixture was stirred for an hour before being transferred to a ceramic plate and dried at 80 °C in an oven to create a PPMA/nanoparticles masterbatch. To prepare the nanocomposites, the masterbatch was combined with the pure PP using HAAK rheomixer 600 OS via melt compounding technique. Typically, the masterbatch and the pure PP were introduced to the HAAK rheomixer at 190 °C and 100 rpm and mixed for 10 min. The resulting nanocomposites were granulated and hot pressed using a carver presser at 200 °C and 10 MPa for 10 min. For each of the nanocomposites developed for this investigation, these steps were repeated. Various nanocomposites were developed with different wt% of the nanoparticles in the PP matrix, which include the pure PP, PP/1wt%GNs, PP/3wt%GNs PP/15wt%BN, PP/1wt%5BN@GN and PP/3wt%BN@GNs.

### 2.4 Evaluation of Materials Properties

Using thermogravimetric analysis (TGA) (TA instrument Q500) the successful functionalization of the nanoparticles was determined in a nitrogen environment at a heating rate of 10 °C/min. Using an X-ray diffractometer (XRD) (X'pert PRO PANalytical) with Cu Kα radiation and a scanning speed of 5°/min, x-ray diffraction patterns of the powder nanoparticles and bulk nanocomposites were examined. The microstructural analysis of the nanoparticles was performed using a transmission electron microscope (TEM) (JEM-2100) at an acceleration voltage of 200 kV and a beam current of 110 µA., The morphologically and microstructurally study of the nanocomposites was done using a scanning electron microscope (SEM) (VEGA 3 TESCAN) at an acceleration voltage of 20 kV. The ASTM G99-95 standard was followed using a tribometer (Anton Paar, TRB3) to analyze the wear behaviors of the nanocomposites. A pin-on-disc dry sliding rotating mode was employed at an applied load of 20 N and a speed of 300 rpm for 15 min. A stainless-steel ball with a radius of 0.3 cm and a roughness of 0.03 µm was used as the counterface. Friction coefficient measurements were made for the nanocomposites. The wear rate (Wr [mm3/Nm]) was measured using a profilometer (Surtronic S128) coupled to the tribometer. Nanoindenter (Anton Paar, NHT) was used to determine the nanomechanical features of the nanocomposites in compliance with ASTM D785 standard. 200 mN load was applied at 20 s penetration, holding and retracting time each. Five to ten tests were performed on each sample and the average results are presented. The nanocomposites' hardness (MPa), elastic modulus (GPa), creep (%) and deformation profile were determined.

## 3 Results and Discussion

### 3.1 TGA and XRD Analyses

Figure 1 represents the TGA result of the pristine and functionalized nanoparticles. It was observed that pristine nanoparticles of GNs and BN have more thermal stability compared to their functionalized counterparts (see Fig. 1a). This deviation is noted to have resulted from the attachment of organic functional groups during functionalization, which reduces their thermal stability. GNs showed a constant thermal stability up to 363 °C, the wt% material's loss at this temperature is attributed to thermal decomposition of oxygen content in GNs. At a temperature of 900 °C, GNs experienced the least thermal stability with a wt% loss of about 10%, this reveals good thermal stability of GNs as reported in other studies [14, 15]. For fGNs, wt% loss started at 82 °C representing the decomposition of water absorbed during functionalization. The second decomposition stage occurred at 160 °C which is due to oxygen from functional groups bonded or reacted with water. Another major weight loss was seen between 700 and 900 °C, this decomposition is attributed to the pyrolytic decomposition of carbon. The highest decomposition is experienced at 900 °C where the fGNs has decomposed with a wt% loss of 36%. BN on the other hand showed good thermal stability up to 900 °C with about 1.5% wt% only. This good thermal stability of BN has been recorded by other researchers [16, 17]. However, fBN showed a drastic decomposition when compared to BN with major decompositions occurring from 50 to

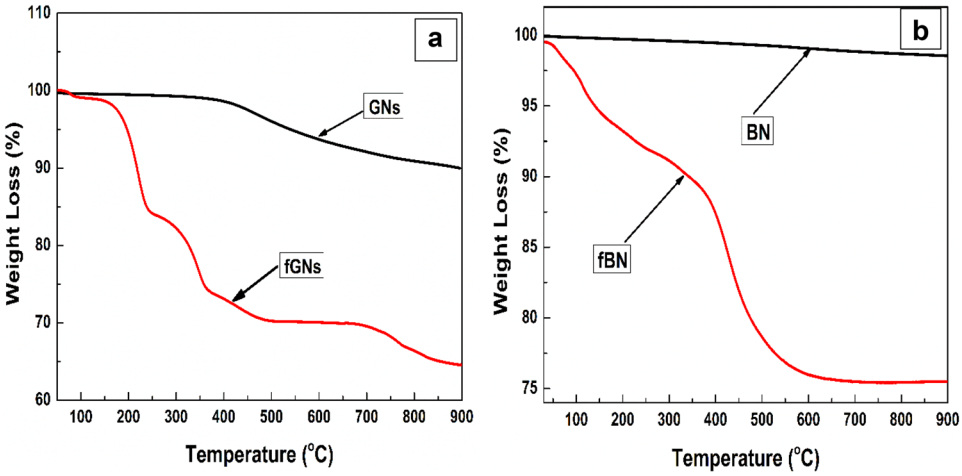


**Fig. 1** TGA Curves of **a** GNs, fGNs and **b** BN, fBN nanoparticles

600 °C as presented in Fig. 1b. The decomposition from 50 to 400 °C is due to remnant water, solvent and oxygen functional groups. At 400–600 °C, the wt% loss resulted from the decomposition of Si–O–Si and Si–O–BN. Between 600 and 900 °C, thermal stability is maintained for fBN as shown in Fig. 1b.

The nanoparticles' and polymer nanocomposites' diffraction patterns are shown in Fig. 2. Graphene has a very high diffraction peak at $2\theta = 26.4°$, which corresponds to the crystal plane of (002) as shown in Fig. 2a. This diffraction peak is the graphitic peak of GNs [18, 19]. In addition, diffraction peaks corresponding to (100) and (004) crystal planes were also present, which occurred at $2\theta = 44.3°$ and 54.5° respectively. On the other hand, BN showed diffraction peaks for hexagonal BN at $2\theta = 26.5°$, 41.4° and 75.8°. These peaks accordingly represent the crystal planes of (002), (100) and (104). For the pure PP, typical diffraction peaks are displayed at $2\theta = 18.6°$, 21.2°, 22.4°, 27.8° and 41.2°, which represent (110), (040), (130), (111) and (060) crystal plane [20, 21] as shown in Fig. 2b. However, the nanocomposites showed only the diffraction peaks corresponding to the PP matrix and GNs/BN nanoparticles, which demonstrate successful incorporation of the nanoparticles in the PP matrix. Hence, no additional diffraction peaks other than those belonging to the nanoparticles were observed, indicating that no new phase was formed in the nanocomposites. In addition to the narrowing of the PP broad peaks by the inclusion of the GNs and BN nanoparticles suggested strong compatibility and interaction between the nanoparticles and the matrix.

## 3.2 Microstructural Investigation

TEM images of the nanoparticles are shown in Fig. 3. The TEM image revealed the successful attachment of BN onto GNs (BN@GNs) as well as the microstructures of the nanoparticles. 2D large in-plane GNs microstructure with smooth surfaces can be seen in Fig. 3a. Figure 3b shows a 2D plate-like image of BN microstructure. Figure 3c shows the incorporation of BN onto GNs (BN@

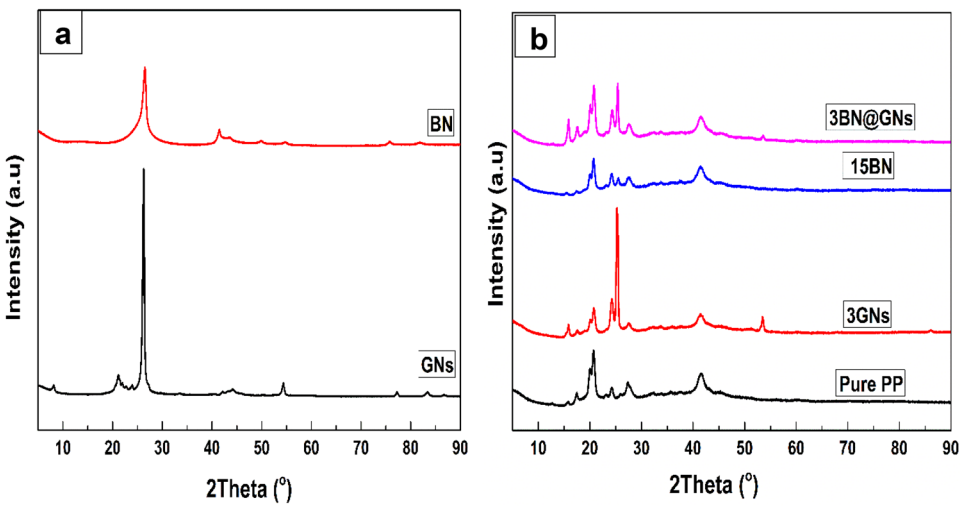


**Fig. 2** XRD diffraction patterns of **a** nanoparticles and **b** nanocomposites

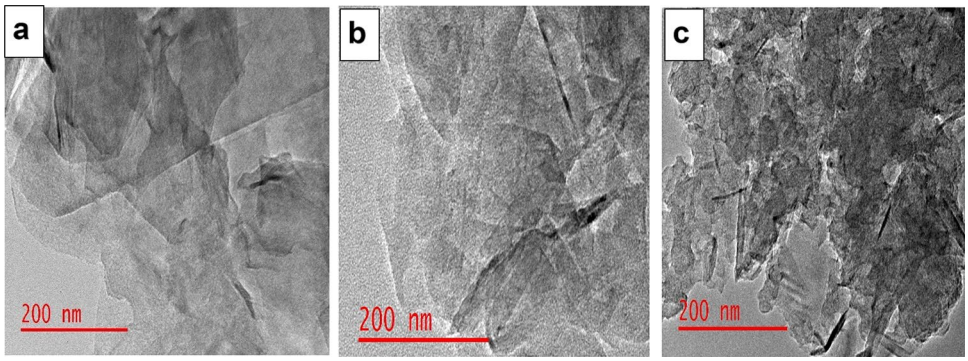


**Fig. 3** TEM micrographs of **a** GNs **b** BN and **c** BN@GNs nanoparticles

GNs), which was achieved through hydrothermal assembly of the nanoparticles. The hydrothermal assembly and interpenetration of GNs and BN could result in a 3D structure. BN@GNs had better dispersion, interlocking, and wettability with PP matrix due to the minimized layers-to-layers interaction of the GNs caused by the presence of BN nanoparticles. This successful interpenetration led to an increase in the anti-wear and nanomechanical properties of PP nanocomposites.

Figure 4 shows the SEM images of the pure PP and its nanocomposites. The pure PP showed a smooth surface due to the absence of external content as presented in Fig. 4a. PP/15wt%BN nanocomposite revealed relatively homogeneous morphology with no significant agglomaration of BN in the PP matrix. This can be credited to the surface functionalization of the nanoparticles, which aided in promoting interfacial bonding between the matrix and the BN nanoparticles. For nanocomposites containing 1wt%GNs and 3wt%GNs as shown in Fig. 4c and d respectivley, there was also relatively good dispersion in the polymer matrix. Earlier reports have shown improvement in the dispersion of GNs in polymer matrix when functionalized [22]. However, the homogeneous microstructure was more pronounced for PP/BN@GNs nanocomposites compared to their counterparts. As earlier stated, the layer-to-layer interactions of GNs in polymer matrix were reduced by the hydrothermal assembly of BN onto GNs (BN@GNs). The resultant SEM images for PP/1wt%BN@GNs and PP/3wt%BN@GNs are shown in Fig. 4. With BN presence, the PP/BN@GNs nanocomposites showed dense microstructure with good dispersion of nanoparticles. As reported in other literature, the functionalization of nanoparticles [23] and mixing with PPMA [24] helped in improving the interrelationship of polymer nanocomposites' constituents. Also, Cui et al. [25] has previouly demostrated that grafting of PPMA onto BN can improve its dispersion with promoted mechnaical properties. This had a significant influence on the improvement of the tribological and nanomechanical properties of polymer nanocomposites.

### 3.3 Wear Behaviour of the Nanocomposites

The wear rates ($W_R$) of the nanocomposites are represented in Fig. 5a. Significantly, all the nanocomposites showed improved $W_R$ compared to the pure PP. This is accountable for the strengthening and hardening of the polymer matrix against detachment during the wear test. This was achieved through the formed network configurations in the matrix and efficient load transfer from the matrix to the nanoparticles, which have good capability to bear the load. The $W_R$ decreased from $24.9 \times 10^{-4}$ $mm^3$/Nm for the pure PP to $2.05 \times 10^{-4}$ $mm^3$/Nm for PP/3wt%BN@GNs, which is about a 91% reduction in the $W_R$ when compared with the pure PP. The significant enhancement in the anti-wear behaviour of the PP/BN@GNs-based nanocomposites is due to the presence of BN, which naturally has a good wear resistance in conjunction with good load bearing of GNs. PP/GNs nanocomposites also showed reduced wear resistance when compared to pure PP, however, the $W_R$ reduction was more pronounced for their PP/BN@GNs counterparts The good wear resistance obtained for the nanocomposites could be attributed to the formation of network structures in the PP matrix through interpenetration of the nanoparticles [26] and their good synergetic effect [22]. However, the PP15wt%BN nanocomposites showed high $W_R$ compared to other nanocomposites. This indicates that more synergy was obtained between GNs and BN in optimal enhancement of the anti-wear property of PP/BN@GNs nanocomposites. The solution blending of the functionalized nanoparticles with the PPMA facilitated their interactions with the PP matrix as revealed by the SEM images, which contributed to the enhanced anti-wear behaviours. It has been previously shown by Chand, Dwivedi [27], that PPMA can enhance the wear response of PP composites reinforced with chopped Jute fibres. Therefore, the promoted bonding and dispersion of the nanoparticles in the PP matrix was a necessity for efficient load transfer, uniform distribution of load among the nanoparticles in the matrix, and enhanced wear resistance of the nanocomposites [28].

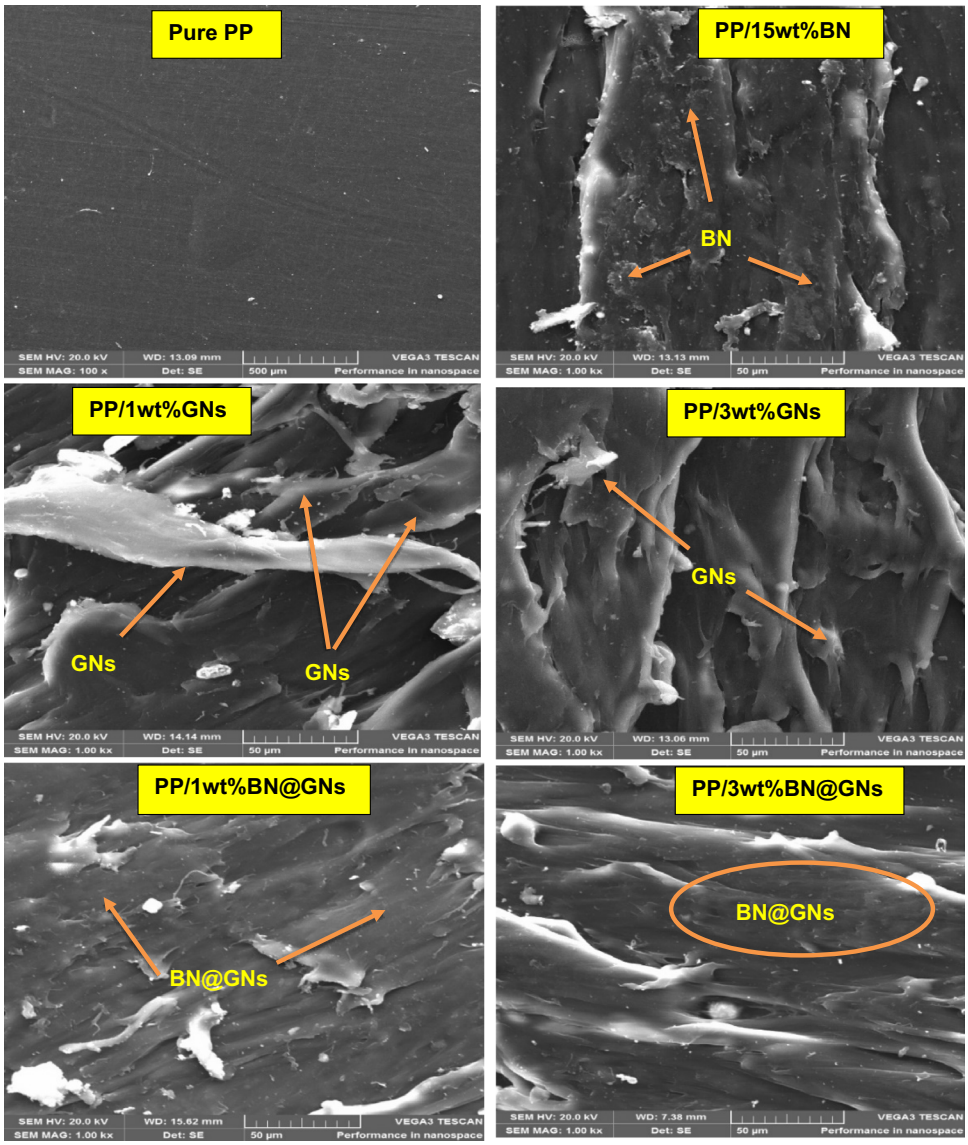


**Fig. 4** SEM Micrographs of the nanocomposites

The coefficient of friction (CoF) of the nanocomposites after the wear test is presented in Fig. 5b. All the nanocomposites showed lower CoF compared to the pure PP. As the friction between the samples and the counterface proceeds, the CoF increases due to abrasive wear. The CoF remained relatively stable or with a slight increase as the frictional test went beyond 200 s due to adhesion wear. Adhesive wear is the wear mechanism that involves the transfer of film from the bulk material under test to the sliding counterface. This prevents direct contact between the materials and the sliding counterface [29]. Hence, it reduces the CoF and detachment of materials as the wear proceeds. However, to achieve this, the transferred film must be thin, uniformly cover the sliding counterface, and strongly adhere to the counterface without peeling off easily [30]. The reduced CoF of the nanocomposites can be attributed to the above-mentioned features, which could not be achieved with the pure PP. Various studies have also reported enhanced wear resistance of GNs-based nanocomposites [22, 29]. In this study, the attachment of BN onto GNs surfaces still maintained relatively low CoF, indicating a good synergetic effect between the nanoparticles [31]. The pure PP revealed higher CoF at all sliding times. The low CoF of the nanocomposites can be credited to the quick dissipation of frictional generated heat from the bulk materials due to the formation of conductive network configurations in the matrix by the nanoparticles. It has been previously demonstrated that high thermal properties materials have good anti-wear behaviours [32]. This is due to their ability to dissipate frictional heat that would have softened the polymer and resulted in a large detachment of materials [10]. The nanocomposites showed smaller wear grooves and lesser peeled transferred film on their wear

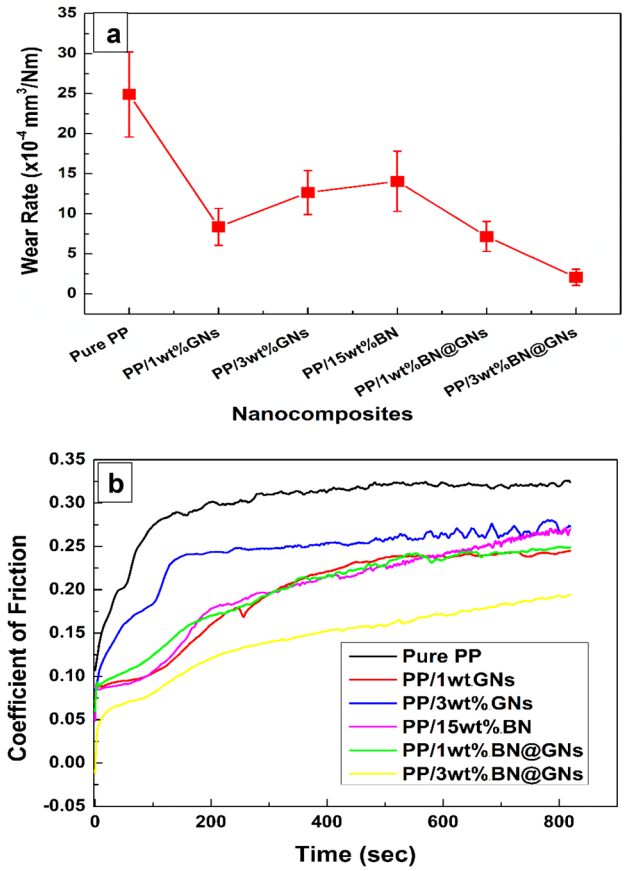


**Fig. 5** **a** Wear rate and **b** Coefficient of friction of the nanocomposites

tracks compared to the pure PP as presented in Fig. 6. This can be attributed to their quick heat dissipation and low softening of the samples. This also suggests the reason for their enhanced wear resistance.

### 3.4 Nanomechanical Properties

Figure 7 represents the nano-hardness (nH) and nano-elastic modulus (nEM) of the nanocomposites. All the nanocomposites showed improved nH when placed side by side with the pure PP as displayed in Fig. 7a. The nH increased from 79.4 MPa for the pure PP to an optimal of about 177.9 MPa for PP/3wt%BN@GNs and a minimum of 130.2 MPa for PP/1wt%GNs. These are about 124% and 64% increases for the former and latter nanocomposites respectively compared to the pure PP. This is an indication of higher resistance to the penetration of the nanoindenter's tip on the nanocomposites compared to the pure PP. It can also be noted that PP/1wt%BN@GNs has lower hardness value compared to other nanocomposites except PP/1wt%GNs, while the same nanocomposite has significantly low wear rate (Fig. 5a). Although materials with low hardness are expected to have high wear rate, elastic modulus also has significant role on the wear response of materials which PP/1wt%BN@GNs has appreciable nEM. For instance, assessment of rigidity and plastic deformation resistance of materials, as per the theory of fracture mechanics, relies on important parameters such as the ratio of hardness to elastic modulus [33], which is useful in the estimation of wear behaviours of wide range of materials [34]. It can be inferred that materials possessing high hardness will exhibit elevated levels of wear resistance. Nevertheless, achieving a balance between hardness and elastic modulus can result in more enhanced resistance to wear.

Since in most cases, an increase in nH often results in to increase in nEM, the nanocomposites also showed higher nEM compared to the pure PP as shown in Fig. 7b. The nEM revealed increment as the GNs content increased from 1 to 3 wt% due to the network structural hardening of the PP matrix by the GNs. However, the PP/15wt%BN showed a drop in the nEM, which can be attributed to lesser hardening and interlocking of the PP matrix since the BN has a lower

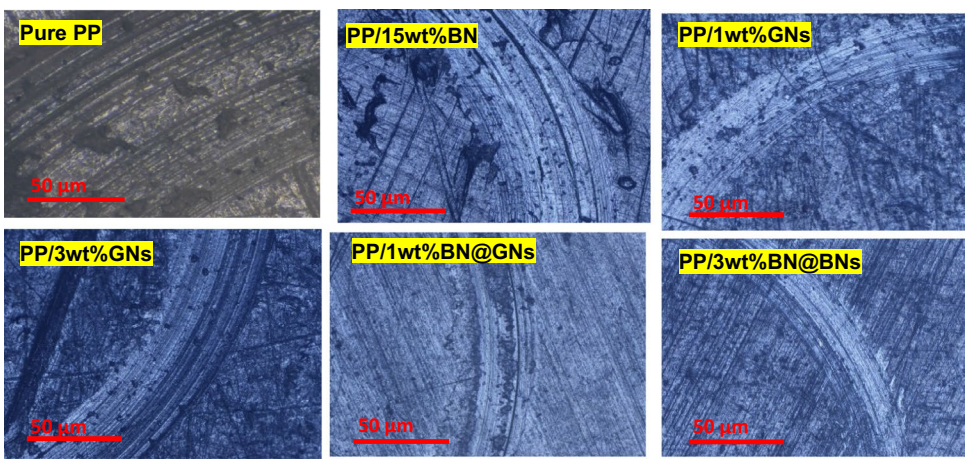


**Fig. 6** Wear Scar on the nanocomposites

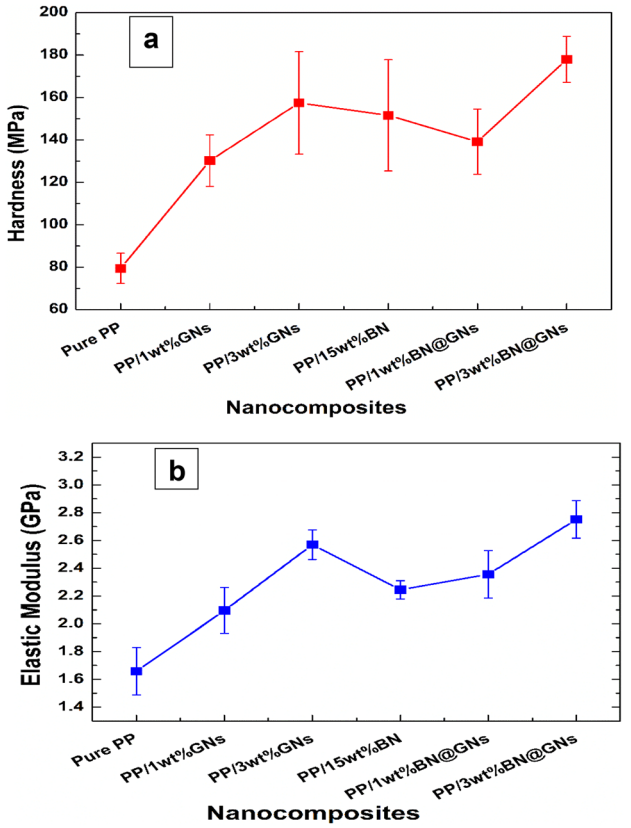


**Fig. 7** **a** Nano-hardness and **b** nano-elastic modulus of the nanocomposites

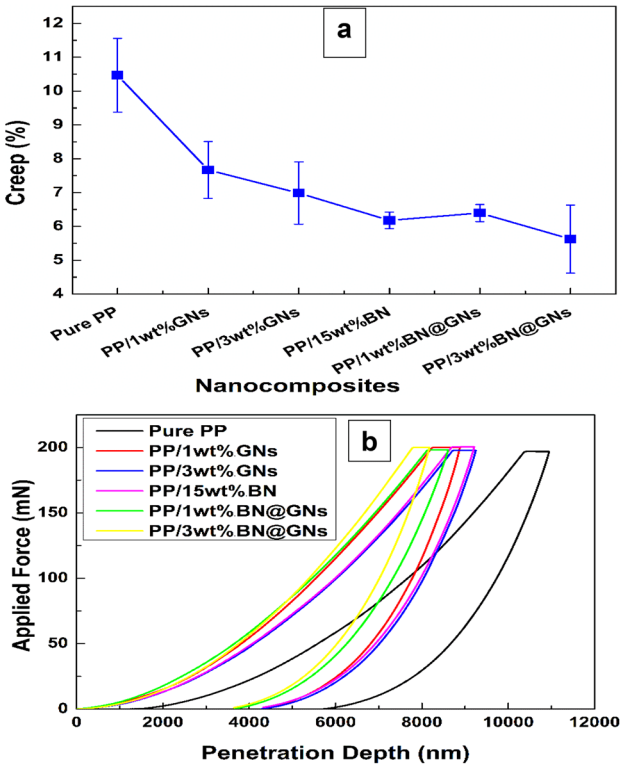


**Fig. 8** **a** Nano-percentage creep and **b** deformation profile of the nanocomposites

aspect ratio compared to GNs, leading to low deformation resistance of the nanocomposite. On the other hand, the nEM increased from 1.66 GPa for the pure PP to an optimal of 2.75 GPa for PP/3wt%BN@GNs nanocomposite, which is about 65.7% increment. Although all the nanocomposites showed significant enhancement in the nH and nEM compared to pure PP, it was more pronounced for the nanocomposite containing 3BN@GNs. The results indicate that on application of load, the sliding of PP chains was restricted and minimized by the nanoparticles in the matrix through mechanical interlocking of the PP chains [35]. Hence, the controlled PP chains' mobility in a restricted manner by the nanoparticles (not allowing the adjacent PP chains to move easily) enhanced the resistance to nanoindentation and plastic deformation of the resultant nanocomposites.

It is worth mentioning that the rough surfaces of BN@GNs as revealed by the TEM image in Fig. 3c facilitated the interlocking of the PP chains, where the presence of the BN served as intermediate layers for effective load transmission. This was deduced from the observation that the nanocomposites containing BN@GNs gave higher values of nH and nEM at similar concentrations with that containing GNs only. Generally, the enhanced nH and nEM can also be accounted for the following reasons; (i) surface functionalities of the nanoparticles, which facilitated their distribution in the matrix [23], (ii) solution mixing to melt compounding route employed in the fabrication process [36], (iii) the use of PPMA, which introduced polar groups in the nanocomposites and enhanced adhesion with their constituents [24], (iv) formation of network structure, which improved the nH and nEM of the nanocomposites through network structural hardening [37] and (v) the good synergy effect among the nanoparticles as this has been previously reported in enhancing properties of polymers [38].

Figure 8a shows that all the nanocomposites have lower nano-percentage creep (nPC) relative to that of the pure PP. This is because the chains of the pure PP were fast-moving or deforming at the constant applied 200 mN load for 20 s. On the other hand, the PP chains in the nanocomposites were slowly moving at similar conditions. This is due to the restrained mobility of the PP chains by the presence of the nanoparticles in the matrix. This resulted in the impediment of the PP chains through network structural hardening. The enhanced nPC of the nanocomposites was more noticeable for PP/3BN@GNs, indicating better PP chains interlocking compared to other nanocomposites. This can be confirmed by the relatively uniform and dense microstructure of the nanocomposite as presented in Fig. 4f. Hence, the PP matrix

was efficiently network hardened by the addition of the BN@GNs nanoparticles [37]. The loading-unloading curves of the nanocomposites are shown in Fig. 8b. The figure shows that the curves for all the nanocomposites shifted to the left compared to that of the pure PP, indicating a reduction in the penetration depth as the applied load was increasing. The reduction in the penetration depth simply means more resistance or difficulty faced by the nanoindenter's tip in penetration into the nanocomposites compared to the pure PP. It means that the nanoparticles in the PP matrix did not allow the PP chains to move easily while the nanoindenter's tip was trying to penetrate. This gave the nanocomposites higher stiffness relative to the pure PP through mechanical interlocking of the PP chains and their restricted mobility or sliding [35]. The restricted polymer chains against movement and interfacial sliding are the ideas for enhancing the mechanical properties of polymers using hard reinforcing fillers, since they are not melted to form hard phases as in the case of most metallic alloys. On the removal of the applied load between 40 and 60 s, the samples tend to restore their original shapes as the penetration depth decreases in that region. From the figure. the penetration depth at 60 s is taken as the final penetration depth ($D_f$), while the maximum penetration depth ($D_m$) is taken at 40 s. The figure shows that the lowest $D_m$ and $D_f$ were recorded for PP/BN@GNs group nanocomposites. This agrees with the large nH and nEM of the nanocomposites.

## 4 Conclusion

The GNs and BN nanoparticles used in this study were first surface functionalized to enhance wettability with each other and good interaction with the PP matrix. The BN was attached to GNs via the hydrothermal assembly method, where the layer-structured BN was stacked on the surfaces of the large in-plane dimensioned GNs. This was revealed by the TEM micrographs. The developed nanocomposites showed reasonable dispersion and good interaction with the PP matrix. The addition of the nanoparticles in the PP matrix promoted its wear resistance. All the developed nanocomposites showed low coefficient of friction (CoF). The wear rate of the nanocomposites was significantly reduced from about 24.9 $10^{-4}$ $mm^3$/mN for the pure PP to a minimum of about $2.05 \times 10^{-4}$ $mm^3$/Nm for PP/3wt%BN@GNs nanocomposite. This is about 91.7% reduction for the nanocomposite relative to the pure PP. The resistance to plastic deformation of the nanocomposites than the pure PP contributed to their enhanced wear resistance. The nanomechanical properties of the nanocomposites obtained from the nanoindentation test showed enhancement. For instance, an optimal of about 124% increase in the nH and 65.7% in the nEM were recorded compared to the pure PP. All the developed nanocomposites showed lower nPC and nanoindenter's tip penetration depth than the pure PP, which indicates higher resistance to plastic deformation.

**Acknowledgements** We appreciate the Faculty of Engineering and the Built Environment and the Centre for Energy and Electric Power, Tshwane University of Technology, South Africa for their supports.

**Author Contributions** UOU: Conceptualization, Methodology, Investigation, Formal Analysis, Writing Original Draft and Project Administration. APIP: Supervision, Funding Acquisition, Review and Editing. OMP: Supervision, Funding Acquisition Resources and Validation and Methodology.

**Funding** Open access funding provided by Tshwane University of Technology.

**Data availability** All data set associated with this study are presented in this article.

## Declarations

**Conflict of Interest** There is no conflict of interest to be declared in this study.



## References

1. Tang Z, Li S (2014) A review of recent developments of friction modifiers for liquid lubricants (2007–present). Curr Opin Solid State Mater Sci 18(3):119–139
2. Quiles-Díaz S, Enrique-Jimenez P, Papageorgiou D, Ania F, Flores A, Kinloch I, Gómez-Fatou MA, Young R, Salavagione HJ (2017) Influence of the chemical functionalization of graphene on the properties of polypropylene-based nanocomposites. Compos Part A Appl Sci Manuf 100:31–39
3. Ike-Eze IE, Uyor U, Aigbodion V, Omah A, Ude S, Daniel-Nkpume C (2019) Tensile and compressive strength of palm kernel shell particle reinforced polyester composites. Mater Res Express 6(11):1–7
4. Mansoori G (2017) An introduction to nanoscience & nanotechnology. In: Ghorbanpour K, Manika A, Varma A (eds) Nanoscience and plant-soil systems. Soil biology series. Springer, Cham
5. Kale R, Potdar T, Kane P, Singh R (2018) Nanocomposite polyester fabric based on graphene/titanium dioxide for conducting and UV protection functionality. Graphene Technol 3:35–46
6. Song H, Li N, Li Y, Min C, Wang Z (2012) Preparation and tribological properties of graphene/poly (ether ether ketone) nanocomposites. J Mater Sci 47:6436–6443

7. Hu K, Kulkarni DD, Choi I, Tsukruk VV (2014) Graphene-Polymer nanocomposites for structural and functional applications. Prog Polym Sci 39(11):1934–1972
8. Wang F, Drzal LT, Qin Y, Huang Z (2015) Mechanical properties and thermal conductivity of graphene nanoplatelet/epoxy composites. J Mater Sci 50:1082–1093
9. Ertuğ B (2013) Powder preparation, properties and industrial applications of hexagonal boron nitride. Sinter Appl 33–55
10. Badgayan ND, Samanta S, Sahu SK, Siva SV, Sadasivuni KK, Sahu D, Sreekanth PR (2017) Tribological behaviour of 1D and 2D nanofiller based high densitypoly-ethylene hybrid nanocomposites: a run-in and steady state phase analysis. Wear 376:1379–1390
11. Songfeng E, Ye X, Wang M, Huang J, Ma Q, Jin Z, Ning D, Lu Z (2020) Enhancing the tribological properties of boron nitride by bioinspired polydopamine modification. Appl Surf Sci 529:147054
12. Madarvoni S, Sreekanth RP (2022) Mechanical characterization of Graphene—Hexagonal Boron Nitride-Based Kevlar–Carbon Hybrid Fabric nanocomposites. Polymers 14(13):2559
13. Jiang F, Cui X, Song N, Shi L, Ding P (2020) Synergistic effect of functionalized graphene/boron nitride on the thermal conductivity of polystyrene composites. Compos Commun 20:100350
14. Liu F, Wu L, Song Y, Xia W, Guo K (2015) Effect of molecular chain length on the properties of amine-functionalized graphene oxide nanosheets/epoxy resins nanocomposites. RSC Adv 5(57):45987–45995
15. Dehghanzad B, Aghjeh MKR, Rafeie O, Tavakoli A, Oskooie AJ (2016) Synthesis and characterization of graphene and functionalized graphene via chemical and thermal treatment methods. RSC Adv 6(5):3578–3585
16. Wu L, Wu K, Lei C, Liu D, Du R, Chen F, Fu Q (2019) Surface modifications of boron nitride nanosheets for poly (vinylidene fluoride) based film capacitors: advantages of edge-hydroxylation. J Mater Chem A 7(13):7664–7674
17. Sudeep PM, Vinod S, Ozden S, Sruthi R, Kukovecz A, Konya Z, Vajtai R, Anantharaman M, Ajayan PM, Narayanan TN (2015) Functionalized boron nitride porous solids. RSC Adv 5(114):93964–93968
18. Ouyang W, Zeng D, Yu X, Xie F, Zhang W, Chen J, Yan J, Xie F, Wang L, Meng H (2014) Exploring the active sites of nitrogen-doped graphene as catalysts for the oxygen reduction reaction. Int J Hydrog Energy 39(28):15996–16005
19. Ramoraswi NO, Ndungu PG (2015) Photo-catalytic properties of TiO2 supported on MWCNTs, SBA-15 and silica-coated MWCNTs nanocomposites. Nanoscale Res Lett 10(1):1–16
20. Jun Y-S, Um JG, Jiang G, Lui G, Yu A (2018) Ultra-large sized graphene nano-platelets (GnPs) incorporated polypropylene (PP)/GnPs composites engineered by melt compounding and its thermal, mechanical, and electrical properties. Compos Part B Eng 133:218–225
21. Yetgin SH (2019) Effect of multi walled carbon nanotube on mechanical, thermal and rheological properties of polypropylene. J Mater Res Technol 8(5):4725–4735
22. Min C, Liu D, Shen C, Zhang Q, Song H, Li S, Shen X, Zhu M, Zhang K (2018) Unique synergistic effects of graphene oxide and carbon nanotube hybrids on the tribological properties of polyimide nanocomposites. Tribol Int 117:217–224
23. Li C-Q, Zha J-W, Long H-Q, Wang S-J, Zhang D-L, Dang Z-M (2017) Mechanical and dielectric properties of graphene incorporated polypropylene nanocomposites using polypropylene-graft-maleic anhydride as a compatibilizer. Compos Sci Technol 153:111–118
24. Orozco VH, Vargas AF, Brostow W, Datashvili T, López BL, Mei K, Su L (2014) Tribological properties of polypropylene composites with carbon nanotubes and sepiolite. J Nanosci Nanotechnol 14(7):4918–4929
25. Cui Z, Martinez AP, Adamson DH (2015) PMMA functionalized boron nitride sheets as nanofillers. Nanoscale 7(22):10193–10197
26. Yu J, Choi HK, Kim HS, Kim SY (2016) Synergistic effect of hybrid graphene nanoplatelet and multi-walled carbon nanotube fillers on the thermal conductivity of polymer composites and theoretical modeling of the synergistic effect. Compos Part A Appl Sci Manuf 88:79–85
27. Chand N, Dwivedi U (2006) Effect of coupling agent on abrasive wear behaviour of chopped jute fibre-reinforced polypropylene composites. Wear 261(10):1057–1063
28. Dike AS, Mindivan F, Mindivan H (2014) Mechanical and tribological performances of polypropylene composites containing multi-walled carbon nanotubes. Int J Surf Sci Eng 8(4):292–301
29. Shen X-J, Pei X-Q, Liu Y, Fu S-Y (2014) Tribological performance of carbon nanotube–graphene oxide hybrid/epoxy composites. Compos Part B Eng 57:120–125
30. Han P, Fan J, Jing M, Zhu L, Shen X, Pan T (2014) Effects of reduced graphene on crystallization behavior, thermal conductivity and tribological properties of poly (vinylidene fluoride). J Compos Mater 48(6):659–666
31. Chen B, Li X, Jia Y, Xu L, Liang H, Li X, Yang J, Li C, Yan F (2018) Fabrication of ternary hybrid of carbon nanotubes/graphene oxide/MoS2 and its enhancement on the tribological properties of epoxy composite coatings. Compos Part A Appl Sci Manuf 115:157–165
32. Mertens AJ, Senthilvelan S (2018) Mechanical and tribological properties of carbon nanotube reinforced polypropylene composites. J Mater Des Appl 232(8):669–680
33. Thangavel E, Ramasundaram S, Pitchaimuthu S, Hong SW, Lee SY, Yoo S-S, Kim D-E, Ito E, Kang YS (2014) Structural and tribological characteristics of poly(vinylidene fluoride)/functionalized graphene oxide nanocomposite thin films. Compos Sci Technol 90:187–192. https://doi.org/10.1016/j.compscitech.2013.11.007
34. Koumoulos EP, Jagdale P, Kartsonakis IA, Giorcelli M, Tagliaferro A, Charitidis CA (2015) Carbon nanotube/polymer nanocomposites: a study on mechanical integrity through nanoindentation. Polym Compos 36(8):1432–1446
35. Yang J, Zhang Z, Friedrich K, Schlarb AK (2007) Creep resistant polymer nanocomposites reinforced with multiwalled carbon nanotubes. Macromol Rapid Commun 28(8):955–961
36. Esawi AM, Salem HG, Hussein HM, Ramadan AR (2010) Effect of processing technique on the dispersion of carbon nanotubes within polypropylene carbon nanotube-composites and its effect on their mechanical properties. Polym Compos 31(5):772–780
37. Bhattacharyya A, Chen S, Zhu M (2014) Graphene reinforced Ultra high molecular weight polyethylene with improved tensile strength and creep resistance properties. Express Polym Lett 8(2):74–84
38. Jyoti J, Babal AS, Sharma S, Dhakate S, Singh BP (2018) Significant improvement in static and dynamic mechanical properties of graphene oxide–carbon nanotube acrylonitrile butadiene styrene hybrid composites. J Mater Sci 53(4):2520–2536